



Article

Vibration Energy at Damage-Based Statistical Approach to Detect Multiple Damages in Roller Bearings

Xiaoqing Yuan ^{1,*} , Naqash Azeem ^{1,2,3,4} , Azka Khalid ⁵ and Jahanzeb Jabbar ⁶¹ School of Mechanical Engineering, Northwestern Polytechnical University, Xi'an 710072, China² The Department of Engineering, University of Naples Parthenope, 80133 Naples, Italy³ Institute of Science and Technology for Sustainable Energy and Mobility (STEMS), CNR, 80133 Naples, Italy⁴ PUNCH Torino S.p.A, 10129 Torino, Italy⁵ Multan College of Arts, Bahauddin Zakariya University, Multan 60000, Pakistan⁶ School of Software and Microelectronics, Northwestern Polytechnical University, Xi'an 710072, China

* Correspondence: yuan@nwpu.edu.cn

Abstract: This study proposes a statistical approach based on vibration energy at damage to detect multiple damages occurring in roller bearings. The analysis was performed at four different rotating speeds—1002, 1500, 2400, and 3000 RPM—following four different damages—inner race, outer race, ball, and combination damage—and under two types of loading conditions. These experiments were performed on a SpectraQuest Machinery Fault Simulator™ by acquiring the vibration data through accelerometers under two operating conditions: with the bearing loader on the rotor shaft and without the bearing loader on the rotor shaft. The histograms showed diversity in the defected bearing as compared to the intact bearing. There was a marked increase in the kurtosis values of each damaged roller bearing. This research article proposes that histograms, along with kurtosis values, represent changes in vibration energy at damage that can easily detect a damaged bearing. This study concluded that the vibration energy at damage-based statistical technique is an outstanding approach to detect damages in roller bearings, assisting Industry 4.0 to diagnose faults automatically.

Keywords: fault detection; Industry 4.0; roller bearings; statistical analysis; vibration energy at damage



Citation: Yuan, X.; Azeem, N.; Khalid, A.; Jabbar, J. Vibration Energy at Damage-Based Statistical Approach to Detect Multiple Damages in Roller Bearings. *Appl. Sci.* **2022**, *12*, 8541. <https://doi.org/10.3390/app12178541>

Academic Editors: Grover Zurita Villarroel and Örjan Johansson

Received: 18 July 2022

Accepted: 24 August 2022

Published: 26 August 2022

Publisher's Note: MDPI stays neutral with regard to jurisdictional claims in published maps and institutional affiliations.



Copyright: © 2022 by the authors. Licensee MDPI, Basel, Switzerland. This article is an open access article distributed under the terms and conditions of the Creative Commons Attribution (CC BY) license (<https://creativecommons.org/licenses/by/4.0/>).

1. Introduction

The maintenance of any machine can be performed using the following three basic techniques: (1) run to failure is the technique in which the maintenance is performed after the part and the analysis of its regions have failed; (2) periodic inspection is focused on determining the time remaining until failure, and maintenance activities are performed according to the schedule prepared by measuring the mean time to when failure last occurred; (3) predictive maintenance is a type of pro-active technique in which the data is acquired continuously, and maintenance activities are performed accordingly; it is focused on performing maintenance before the failure happens [1]. In the mechanical industry, bearings have a vital role, as they support the shaft and bear a greater loading. Early stage detection of bearing faults is critical in order to avoid catastrophic failure. Hence, predictive maintenance is very often used in many branches of industry. Industry 4.0 has currently become popular, and predictive maintenance can be a very helpful tool in making it fully automatic. Some developed technologies, such as cloud computing, the Internet of things, and big data analytics, have already provided many benefits for the implementation of Industry 4.0 [2]. The strain sensor based on the highly sensitive nanocomposite is developed for Industry 4.0 [3]. To implement Industry 4.0, a review for sensor monitoring is also presented [4]. However, big data and cyber-physical systems require more attention in Industry 4.0 to make it fully autonomous [5].

Numerous studies were conducted to diagnose faults in rotating machinery. Experimental analysis was performed to detect damages in a wind turbine. The vibration signals

were measured by mounting the strain gauges on the gearbox and generator. Both the analyses based on the time domain and frequency domain were performed to capture components' features and find the location of the damages [6]. A novel method, called extended phase space topology (EPST), was proposed for pattern recognition and machinery diagnostics. The EPST was applied to the vibration data obtained from a rotating machine through the proximity probes. The EPST does not require any feature selection; therefore, it is easily applied in an automated process [7]. The different fault conditions in rotating machinery were identified using an efficient feature extraction technique on the raw vibrational signal so that the mechanical health status can be detected in a timely manner. The proposed feature extraction technique was based on improved multiscale dispersion entropy (IMDE) and max-relevance min-redundancy (mRMR). The proposed methodology was analyzed experimentally, and the results proved that it is a useful technique for the fault diagnosis of mechanical components, including gearboxes and rolling bearings [8].

The roller bearing diagnosis was performed at the low-energy stage of its development. The information from a machine vibration signal was extracted by amplitude level-based decomposition of the signal, and the spectral analysis was performed to extract features for bearing damage [9]. The diagnosis for a rolling element bearing was also studied using a new fault feature extraction method—decomposing the vibration signal with adaptive local iterative filtering (ALIF) and measuring the signal complexity with modified fuzzy entropy. The technique was experimentally checked, and the results concluded that the proposed technique can be used in fault diagnostics [10]. The bearing damages were also analyzed using vibrational resonance (VR) on the vibrational signals generated through simulation and experimentation. The proposed methodology was compared with the envelope spectrum, and it was concluded that the proposed VR method is better than the envelope spectrum method because the characteristic frequency was remarkably amplified in the proposed VR methodology [11]. After reviewing the approaches for the change detection and optimal segmentation of the vibrating data acquired through the operation of the rolling element bearings (REB), a new approach based on the change detection and optimal segmentation of the vibrating signal was presented, and it was concluded that the proposed technique can be used for condition monitoring and industrial processes [12]. The importance of correlated kurtosis was explored to indicate the periodicity and the impact of the signal [13]. A novel method based on data-driven random fuzzy evidence acquisition and the Dempster–Shafer evidence theory was introduced to diagnose faults in rolling bearings, and the results proved that it has high accuracy [14]. The bearing faults were also detected by combining fuzzy entropy of empirical mode decomposition (EMD), principal component analysis (PCA), and the self-organizing map neural network [15]. An improved pattern spectrum algorithm based on a support vector machine was proposed to extract features by employing a morphological erosion operator. The experimental results concluded that the accuracy of the proposed algorithm reached 87.5% (21/24) in training and 91.7% (44/48) in testing [16]. The deep structure of the convolutional neural network (CNN), which does not require the extraction of features and still shows high classification accuracy, was proposed to diagnose the bearing faults [17].

Whenever a mating surface hits a defect, the energy is converted from kinetic into elastic potential energy. A shock pulse is generated at the interface because of a sudden change in the contact stress. These sudden changes (shock pulses) excite the system components, which react in their normal modes [18]. Machinery defects can easily be detected in the early stages with periodically repeating shocks; gear defects have been detected with the real order derivative [19]. The stochastic aspect of the shock occurrence was discovered for first time by the author's of [20], in which these shock pluses were analyzed on simulated and actual vibration data by modeling the bearing fault vibration as a series of impulse responses of a single degree of freedom system. These findings were readdressed in their subsequent works [21–23]. In another article, bearing clearance has been determined by using three methods, including the calculation of the spectral kurtosis of corresponding spectra, and the results showed reliability in service detection [24].

Predictive maintenance have proven effective for Industry 4.0 because it provides maintenance activities before the failure happens. In order to perform predictive maintenance, accurate condition monitoring of mechanical machinery is required. This article proposes that due to the impairment in a damaged bearing, the bearing produces high amplitude vibrations as compared to the undefective bearing. The damaged bearing has high vibration energy at damage, which is why it produces high amplitude vibrations. The proposed method has been examined through systematic and detailed experimentation.

The literature concluded that the concept of Industry 4.0 requires some automatic fault detection techniques for implementation. This research article proposes two statistical parameters, histograms and kurtosis, as the indications of a change in vibration energy at damage for the detection of roller bearing faults. The damaged bearing will produce high vibrations, as it has high damage energy, and this damage energy change can be used to detect faults in the roller bearing. Detailed experimentation is performed to explore the proposed methodology. An overview of the vibration energy at damage concept and corresponding formulas are given in the next section, followed by the experimental setup section, in which the experimental setup is explained in detail. Finally, the results are discussed.

2. Vibration Energy at Damage-Based Statistical Approach

One body has six degrees of freedom (DOF): three are translational, and three are rotational. The equation of motion for a shaft under torsional/rotational vibration is shown by Equation (1). The signal acquired from the machine in terms of displacement, velocity, or acceleration can be compared with a defected signature to perform fault diagnosis.

$$I\ddot{\theta} + K_d\dot{\theta} + K_t\theta = T(t) \quad (1)$$

where I is the mass moment of inertia, $\ddot{\theta}$ is the angular acceleration, $K_d\dot{\theta}$ is the damping coefficient in the torsional domain, $K_t\theta$ is the torsional stiffness, and $T(t)$ is the torque as a function of time. These torsional vibrations can be measured by a laser torsional vibrometer and optical encoders. In this study, accelerometers were used to measure rotational vibration, rather than measuring the torsional vibration. The data can be acquired in terms of displacement (x), velocity (\dot{x}) or acceleration (\ddot{x}). The followings are the basic parameters to measure vibration:

$$|x| = X \quad , \quad |\dot{x}| = \omega X \quad , \quad |\ddot{x}| = \omega^2 X \quad (2)$$

where ω is the rotational frequency in rad/s, which can also be expressed as $2\pi f$, and f is the frequency in cycles per second, or hertz (Hz). Generally, the X is measured at $0 < f < 10$, the ωX is measured at $10 < f < 1000$, and the $\omega^2 X$ is measured at $f > 1000$. On the right hand side of the equation of motion, there is a forcing function, and it depends upon ω , which is the forcing frequency. The natural characteristics of the machine can be obtained from Equation (3):

$$\omega_n = \sqrt{\frac{k}{m}} \quad f_n = \frac{1}{2\pi} \sqrt{\frac{k}{m}} \quad (3)$$

where ω_n , k , m , and f_n are the natural rotational speed, stiffness, mass, and natural frequency of the machine, respectively. The resonance will occur if the forcing frequency is equal to the natural frequency, and it will result in larger displacement. Operators avoid the natural frequency during the operation, but this parameter is calculated by designers for safety. The following Equations (4) and (5) explain the frequency response functions, where F is the forcing function:

$$Stiffness = \frac{F}{x} \quad Damping = \frac{F}{\dot{x}} \quad Mass = \frac{F}{\ddot{x}} \quad (4)$$

$$Compliance = \frac{x}{F} \quad Mobility = \frac{\dot{x}}{F} \quad Impedance = \frac{\ddot{x}}{F} \tag{5}$$

In this study, a statistical approach is proposed to detect roller bearing damages. As the roller bearings are mainly used in industry, it is important to detect damages at the early stages. The roller bearings have to bear great loading at high rotating speeds. Therefore, it is necessary to use a proactive technique for inspection. This technique not only provide a safe environment the proper function of the machines, but it also decreases the maintenance costs. Basically, the roller bearings bear loading with their rolling elements and reduce friction. Roller bearings have three main components: the balls, the inner race, and the outer race.

The disorder or sudden peak in the vibration-based frequency or time domain data are often considered faults. Because, as the ball passes through a discontinuity or defect, it can be subjected to an impulsive force as an effect of damages, peaks in courses of physical magnitudes can be noticed. Thus, most of the researchers have analyzed characteristic features of signals at frequency. In this research, the characteristic fault frequency multipliers for ball pass frequency outer race (*BPFO*), ball pass frequency inner race (*BPFI*), ball spin frequency (*BSF*), and fundamental train frequency (*FTF*) were calculated using Equations (6)–(9). However, our main objectives are to plot histograms and calculate kurtosis values so that the damage energy for an intact bearing and damaged bearing can be compared.

$$BPFO = \frac{n}{2} \left[1 - \frac{D_B}{D_P} \cos \theta \right] \tag{6}$$

$$BPFI = \frac{n}{2} \left[1 + \frac{D_B}{D_P} \cos \theta \right] \tag{7}$$

$$BSF = \frac{D_P}{2D_B} \left[1 - \left(\frac{D_B}{D_P} \right)^2 \cos^2 \theta \right] \tag{8}$$

$$FTF = \frac{1}{2} \left[1 - \frac{D_B}{D_P} \cos \theta \right] \tag{9}$$

where, D_B is the ball diameter, D_P is the pitch diameter, n is the number of balls, and θ is the angle of contact. The ER-16K faulty rolling element bearings, with ball diameter $D_B = 8$ mm and pitch diameter $D_P = 38$ mm, number of balls $n = 9$, and angle of contact $\theta = 9.08^\circ$, are used in this study. By putting the values of D_B , D_P , n , and θ in the above Equations (6)–(9), the characteristic fault frequencies of the roller bearings are calculated and shown in Table 1.

Table 1. The characteristic fault frequency multipliers of roller bearings used in this study.

Operating Speed RPM	Ball Pass Frequency Outer (BPFO)	Ball Pass Frequency Inner (BPFI)	Ball Spin Frequency (BSF)	Fundamental Train Frequency (FTF)
	3.572	5.43	2.322	0.402
1002	3579.144	5440.86	2326.644	402.804
1500	5358	8145	3483	603
2400	8572.8	13,032	5572.8	964.8
3000	10,716	16,290	6966	1206

The characteristics fault frequencies are obtained by multiplying the operating speed by the multipliers calculated in the second row of Table 1. The peaks at these characteristics fault frequencies and their respective harmonics are analyzed, and the bearing is often regarded as a damaged bearing if the vibrations are high at these characteristics fault frequencies (BPFO, BPFI, BSF, and FTF). However, in reality, these peaks are submerged by the noise, and it is not an easy task to recognize the peaks at these characteristic fault

frequencies. Thus, a novel method is proposed in this study, based on the vibration energy at damage. The histograms, along with the kurtosis values, were used to analyze the vibration data of an intact and damaged bearing. The kurtosis is a measurement of the frequency of extreme values, or peakedness of distribution. The kurtosis (K) can be calculated from the following Equation (10):

$$K = \frac{m_4}{m_2^2} = \frac{m_4}{(\sigma^2)^2} \tag{10}$$

where m_4 is the fourth moment, m_2 is the second moment, and σ is the variance. First, the deviation from the mean is calculated by using Equation (11), then the second moment (m_2), variance (σ), and the fourth moment (m_4) can be calculated from Equations (12)–(14), respectively. The averaged value of kurtosis is used in this study so that the accuracy of measurement can be improved. The averaged value of kurtosis is the mathematical average of the numeric (absolute) value of all data blocks.

$$\text{deviation from the mean} = X_i - X_{avg} \tag{11}$$

$$m_2 = \frac{\sum_{i=1}^n (X_i - X_{avg})^2}{n} \tag{12}$$

$$\sigma^2 = \frac{\sum_{i=1}^n (X_i - X_{avg})^2}{n} \tag{13}$$

$$m_4 = \frac{\sum_{i=1}^n (X_i - X_{avg})^4}{n} \tag{14}$$

where, X_i is the i th observation, X_{avg} is the arithmetic average of all values, and n is the number of values. The formula to calculate the second moment (m_2) and variance (σ) is the same. Finally, the formula to calculate kurtosis (K) becomes:

$$K = n \times \frac{\sum_{i=1}^n (X_i - X_{avg})^4}{\left(\sum_{i=1}^n (X_i - X_{avg})^2\right)^2} \tag{15}$$

The system that samples the data from a machine and then converts it to the digital form is known as the data acquisition system (DAQ). The following Equations (16)–(19) are used in DAQ:

$$T = N \times \Delta t \tag{16}$$

$$f_s = 2 f_{max} \tag{17}$$

$$\Delta f = \frac{1}{T} = \frac{1}{N \times \Delta t} = \frac{f_s}{N} \tag{18}$$

$$\text{Seconds per block} = \frac{\text{Rows per block}}{\text{Sampling rate}} \tag{19}$$

where T is the total time, N is the number of data points, Δt is the time resolution, f_s is the sampling frequency, f_{max} is the maximum frequency, and Δf is the frequency resolution. The smaller the time resolution is, the higher the sampling frequency will be, and this will enhance the results. By increasing the f_{max} , speed range, and spectrum lines, the frequency resolution can be enhanced. Generally, the f_{max} is calculated by 20 or 40 times the rotating speed. The Hanning window produces a high-frequency resolution, along with protection from leakage, with fair amplitude accuracy.

3. Experimental Setup

This study is based on the experiments performed on a machinery fault simulator (MFS). Experiments testing the vibration energy at damage-based statistical approach

in detecting bearing damages were performed on an MFS made by SpectraQuest. This simulator has a three-phase pre-wired electric motor of 1 HP that drives a rotor assembly with a variable frequency AC drive that has a multi-featured, front panel programmable controller. The rotating speed is measured by a built-in tachometer, with an LCD display, that can be varied from 0 to 6000 rpm with a short duration. The motor and rotor shaft is connected with an L-type standard jaw coupling, made of sintered iron, that has a length of 54.6 mm. The rotor assembly consists of a 25.4 mm diameter turned, ground, and polished (TGP) steel rotor shaft supported by two roller bearings. The roller bearings are placed in a horizontal-type split bracket. The accelerometers are placed on inboard and outboard bearing housings in the vertical and horizontal direction, and the vibration data are recorded. These accelerometers can record the vibration with a sensitivity of 10.2 mV and a measurement range of $\pm 490 \text{ ms}^{-2}$. An eight-channel data acquisition card was used to acquire the data from the simulator, which was later analyzed. The complete experimental apparatus is shown in Figure 1.

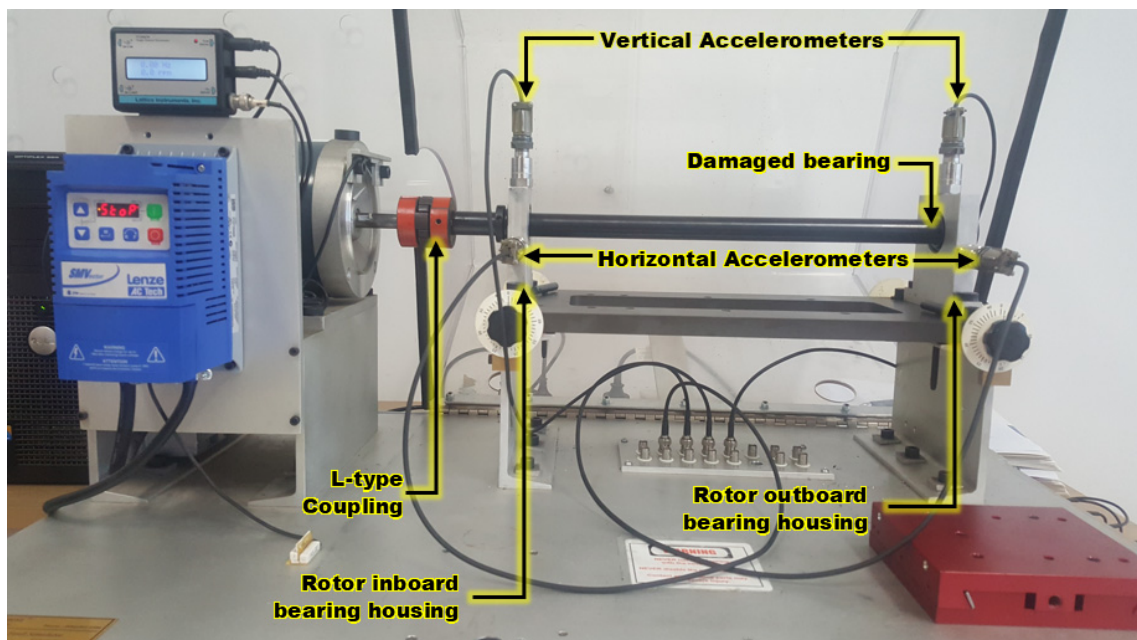


Figure 1. Experimental setup for evaluating bearing damages.

This simulator was used in our previous studies to detect: the imbalance caused by using accelerometers at three different operating speeds [25], the misaligned and cracked shafts using order analysis [26], the bearing faults using spectral density analysis [27] and octave analysis [28]. It was also used to detect imbalance using piezoelectric strain sensors [29]. The misaligned and cracked shaft was also analyzed on this simulator, and sensitive locations for transducers were discussed [30]. This study focuses on multiple damages in roller bearings; bearing damages have been analyzed by comparing the intact bearing's histogram and kurtosis values with the following defected bearings: (1) inner race defect; (2) outer race defect; (3) ball defect; and (4) combination defect.

All of the above defected bearings in this experimental study were used at 1002, 1500, 2400, and 3000 RPM rotating speeds, with two types of loading conditions: without installing a bearing loader and with installing a bearing loader. In the first type of the loading condition, the vibration data of intact and defected bearings were acquired through the accelerometers, without installing a bearing loader on the rotor assembly. In the second type of loading condition, a bearing loader was installed at a distance of 5 cm from the outboard bearing housing, and the vibration data of intact and defected bearings were acquired through the accelerometers. For both types of loading conditions, the defected

bearing was placed at outboard bearing housing. The intact bearing histograms and kurtosis values are compared with each defected bearing. The inner race, outer race, ball, and combination damage bearings were placed only at the outboard bearing housing. The vibration data were acquired with 12,800 spectral lines and 10 kHz maximum frequency.

The overall velocity-RMS values have been collected at no fault condition for both types of loading conditions in order to follow the ISO standard 20816-1 [31]; this was also done in our previous studies [25–28]. The ISO standard 20816-1 has a vibration severity chart consisting of four categories: A, B, C, and D. Category ‘A’ means that the machine is in outstanding condition, and category ‘D’ means that the machine’s vibrations are not permissible. The vibration severity chart of ISO standard 20816-1 also classifies all machines into four classes, class I through class IV, depending upon the size of the machine. The simulator had a power of 1 HP and according to the ISO standard 20816-1 vibration severity chart, it belongs to class 1. The velocity-RMS values in class 1 range from 0.28 mm/s to 2.80 mm/s for category ‘A’ to ‘C’, respectively, meaning that if the machine belongs to category ‘C,’ the vibrations are within the limits. The velocity-RMS values before placing the damaged bearings for all rotating speeds, without installing a bearing loader and with installing a bearing loader, are shown in Tables 2 and 3 respectively. From Tables 2 and 3, it is found that the maximum overall velocity-RMS value is 2.7166 mm/s in the horizontal direction at 3000 RPM for the rotor inboard bearing housing, which is less than the 2.80 mm/s value of category ‘C’. Therefore, this simulator falls into category ‘C,’ meaning that the vibrations are within tolerable limits, and the experiments can be performed.

Table 2. Overall velocity-RMS (mm/s) without installing a bearing loader at no-fault condition.

Rotating Speed (RPM)	Rotor Inboard Bearing Housing		Rotor Outboard Bearing Housing	
	Horizontal	Vertical	Horizontal	Vertical
1002	0.2757	0.1337	0.2771	0.1741
1500	0.5939	0.3116	0.6544	0.5724
2400	1.2863	0.7680	1.2607	1.0588
3000	2.0655	1.1951	2.6264	2.3558

Table 3. Overall velocity-RMS (mm/s) with installing a bearing loader at no-fault condition.

Rotating Speed (RPM)	Rotor Inboard Bearing Housing		Rotor Outboard Bearing Housing	
	Horizontal	Vertical	Horizontal	Vertical
1002	0.3557	0.1557	0.2675	0.1548
1500	0.6291	0.2669	0.4674	0.2990
2400	1.1643	0.9012	0.7484	0.5704
3000	2.7166	1.5035	1.7238	1.4493

4. Results and Discussion

The four types of bearing damages: inner race, outer race, ball, and combination damage, were analyzed by using histograms and kurtosis values in the following sections.

4.1. Inner Race Damage

A bearing with an inner race fault was replaced with an intact bearing at the outboard bearing housing. The accelerometers were installed on the outboard and inboard bearing housing in the horizontal and vertical direction. To analyze the inner race defect, the simulator was operated at 1002, 1500, 2400, and 3000 RPM rotating speed, and the data were acquired with two loading conditions: (1) without installing a bearing loader, and (2) with installing a bearing loader. The histograms for the outboard bearing housing in the vertical direction at each rotating speed for intact and inner race bearing damage were compared, without installing a bearing loader and with installing a bearing loader, as shown in Figures 2 and 3, respectively. The kurtosis values for the outboard bearing

housing in the vertical direction at each rotating speed, without installing a bearing load and with installing a bearing loader, are shown in Table 4.

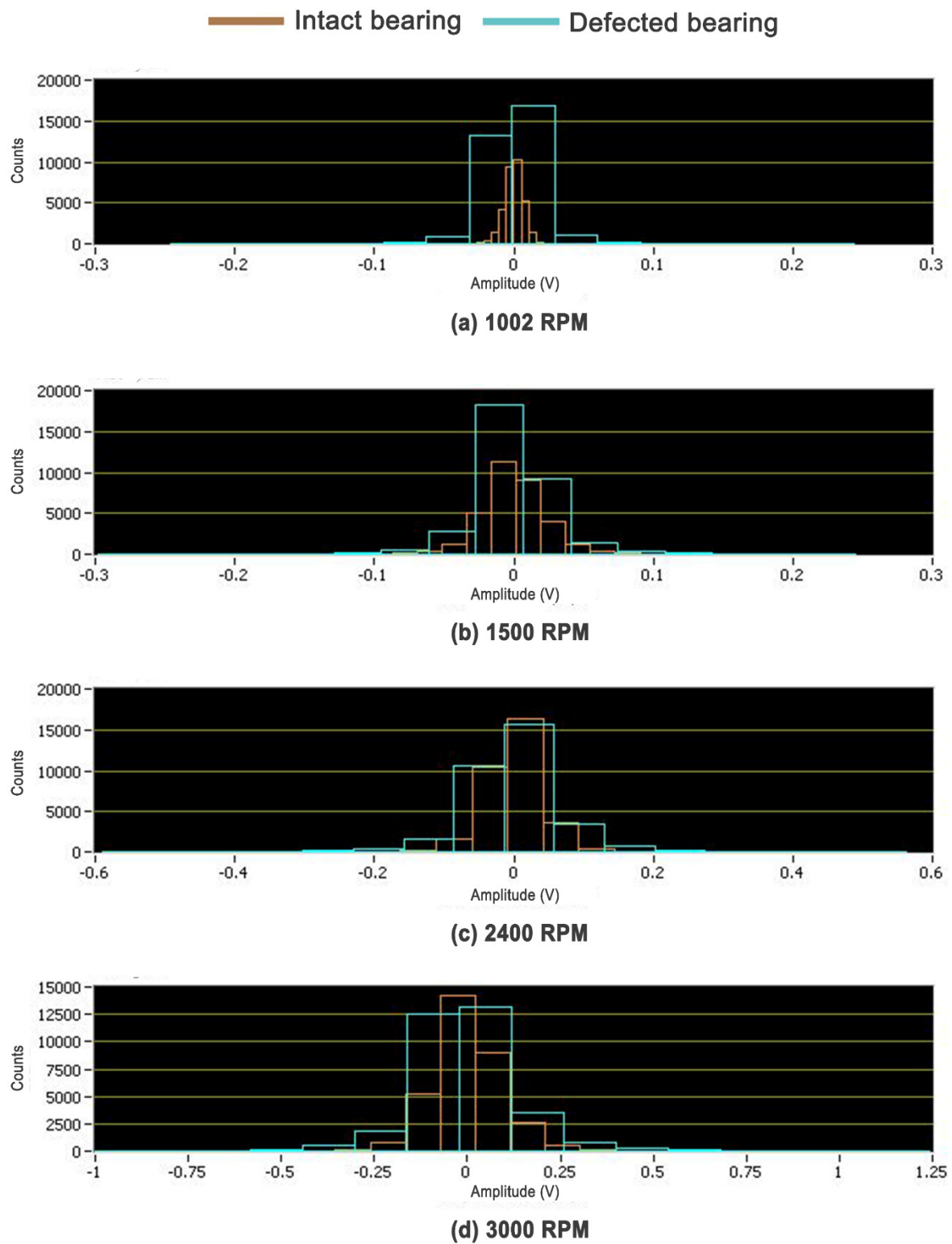


Figure 2. Histograms for an inner race damaged bearing without installing a bearing loader.

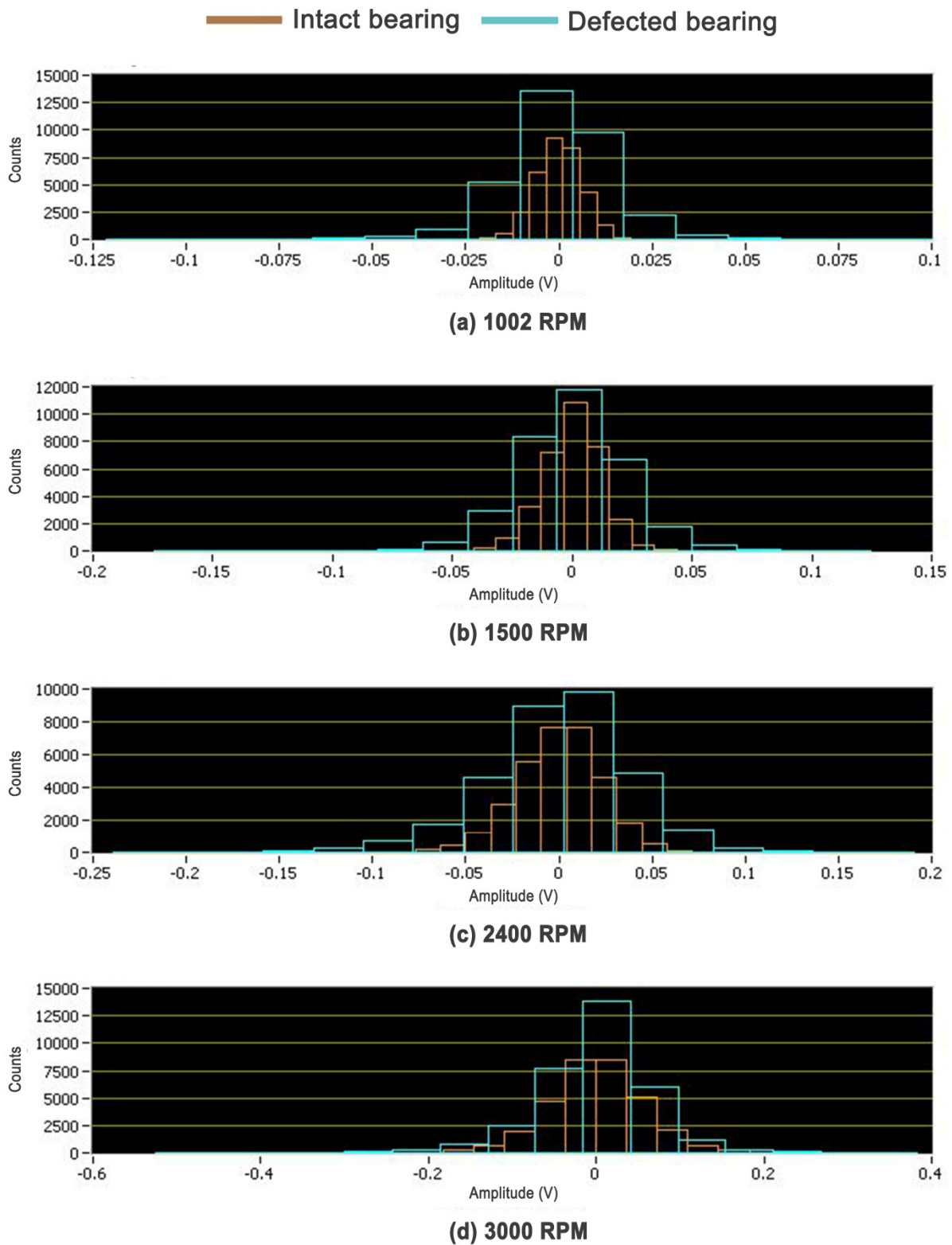


Figure 3. Histograms for an inner race damaged bearing with installing a bearing loader.

From Figures 2 and 3, it can be seen that the bars are high for an inner race damaged bearing for both of the loading conditions. At all rotating speeds, the frequency of the inner race damaged bearing data is high as compared to the intact bearing data. The kurtosis values shown in Table 4 are also high in the case of an inner race damaged bearing for all rotating speeds. As the kurtosis values give a better idea of vibration energy at damage;

therefore, the histograms and kurtosis values concluded that the energy at damage-based approach is an efficient way to detect inner race damage in the rolling bearing.

Table 4. Averaged kurtosis values for an inner race defect.

Rotating Speed (RPM)	Without Installing a Bearing Loader		With Installing a Bearing Loader	
	Intact Bearing	Damaged Bearing	Intact Bearing	Damaged Bearing
1002	2.319673	10.890377	1.609728	3.221563
1500	2.518273	4.783087	1.803017	2.406770
2400	4.293731	4.232281	1.659314	2.114533
3000	2.661141	4.211987	1.920782	3.395726

4.2. Outer Race Damage

In order to analyze the outer race damage, an outer race damaged bearing was placed, and the intact bearing was removed from outboard bearing housing. The vibration data were acquired through accelerometers at 1002, 1500, 2400, and 3000 RPM rotating speed. The histograms for all rotating speeds, without installing a bearing loader and with installing a bearing loader, were formulated. The intact bearing and outer race damaged bearing’s histogram in the vertical direction of the outboard bearing housing were compared without installing a bearing loader and with installing a bearing loader, and the results are presented in Figures 4 and 5, respectively. The kurtosis was also calculated at each rotating speed, without installing a bearing loader and with installing a bearing loader, in the vertical direction of the outboard bearing housing, as shown in Table 5.

Table 5. Averaged kurtosis values for an outer race defect.

Rotating Speed (RPM)	Without Installing a Bearing Loader		With Installing a Bearing Loader	
	Intact Bearing	Damaged Bearing	Intact Bearing	Damaged Bearing
1002	2.319673	5.728271	1.609728	2.449496
1500	2.518273	3.234788	1.803017	2.350686
2400	4.293731	2.457544	1.659314	2.953900
3000	2.661141	2.400164	1.920782	2.522863

The vibration data for an outer race damaged bearing are more scattered as compared to those for the intact bearing, since the width and height of the bars for an outer race damaged bearing are greater in Figures 4 and 5. The outer race damage is significantly visible in histograms for all rotating speeds and for both of the loading conditions. The bars are high for an outer race damaged bearing because the damaged bearing produces high vibrations, as it has high damage energy. The kurtosis values are also high for an outer race damaged bearing, as shown in Table 5, except at 2400 RPM without installing a bearing loader; this may be due to nonlinearities of the simulator. The histograms, along with the kurtosis values, revealed that this is an effective approach in detecting an outer race damage in the rolling bearing.

4.3. Ball Defect

These experiments were performed by replacing the intact bearing at outboard bearing housing with a bearing that has damaged balls. The ball damaged experiments were performed at 1002, 1500, 2400, and 3000 RPM rotating speed. The intact bearing’s histogram and ball damaged bearing’s histograms were computed at each speed on the vibration data recorded with the help of accelerometers mounted on the inboard bearing housing and outboard bearing housing in the horizontal and vertical direction. The vertical direction histograms at the outboard bearing housing for intact and ball damaged bearing are only shown without installing a bearing loading and with installing a bearing loader in Figures 6 and 7, respectively. At each rotating speed, the kurtosis values were computed in both directions,

but only the horizontal direction kurtosis values are shown in Table 6, as this shows the ball damage more clearly.

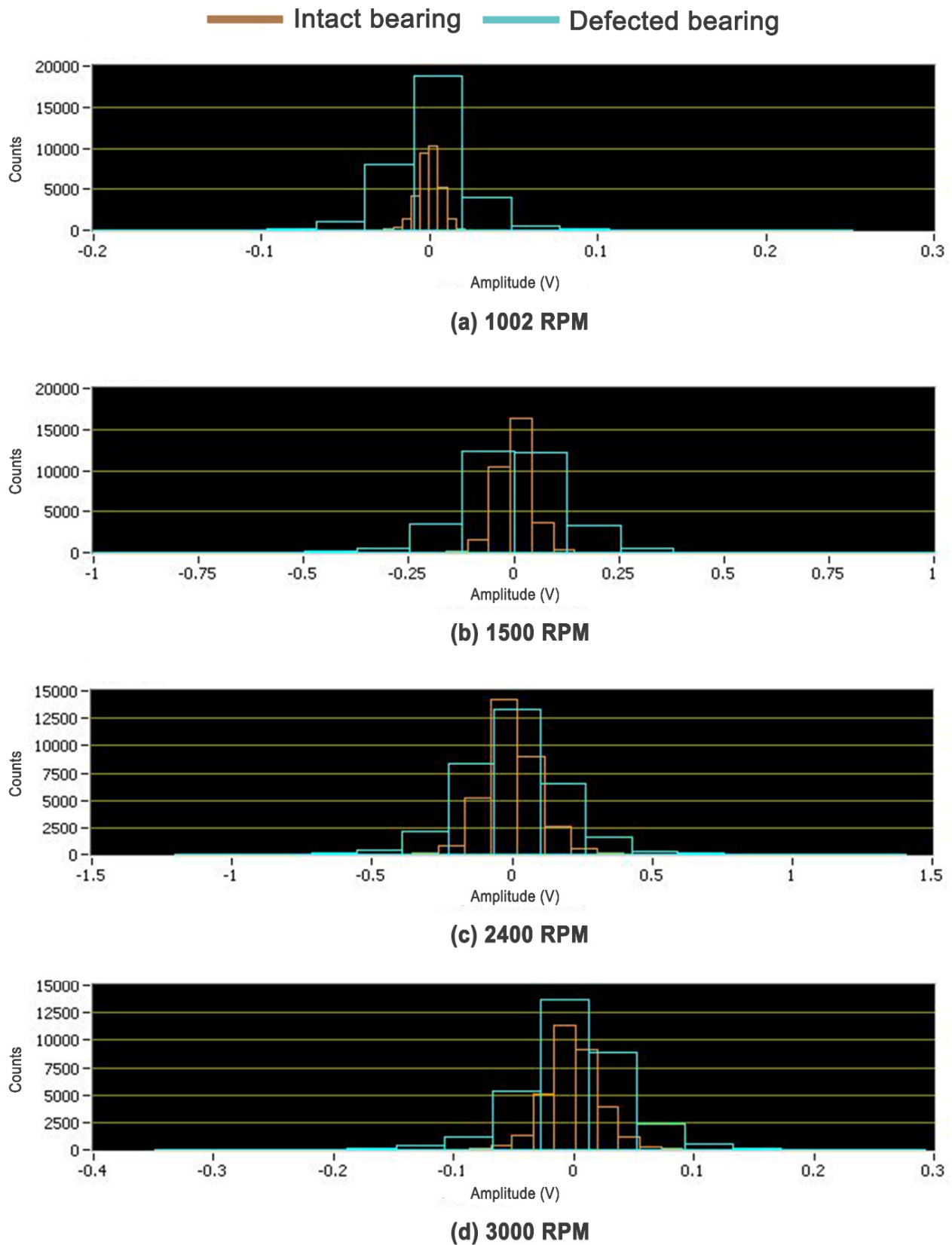


Figure 4. Histograms for an outer race damage without installing a bearing loader.

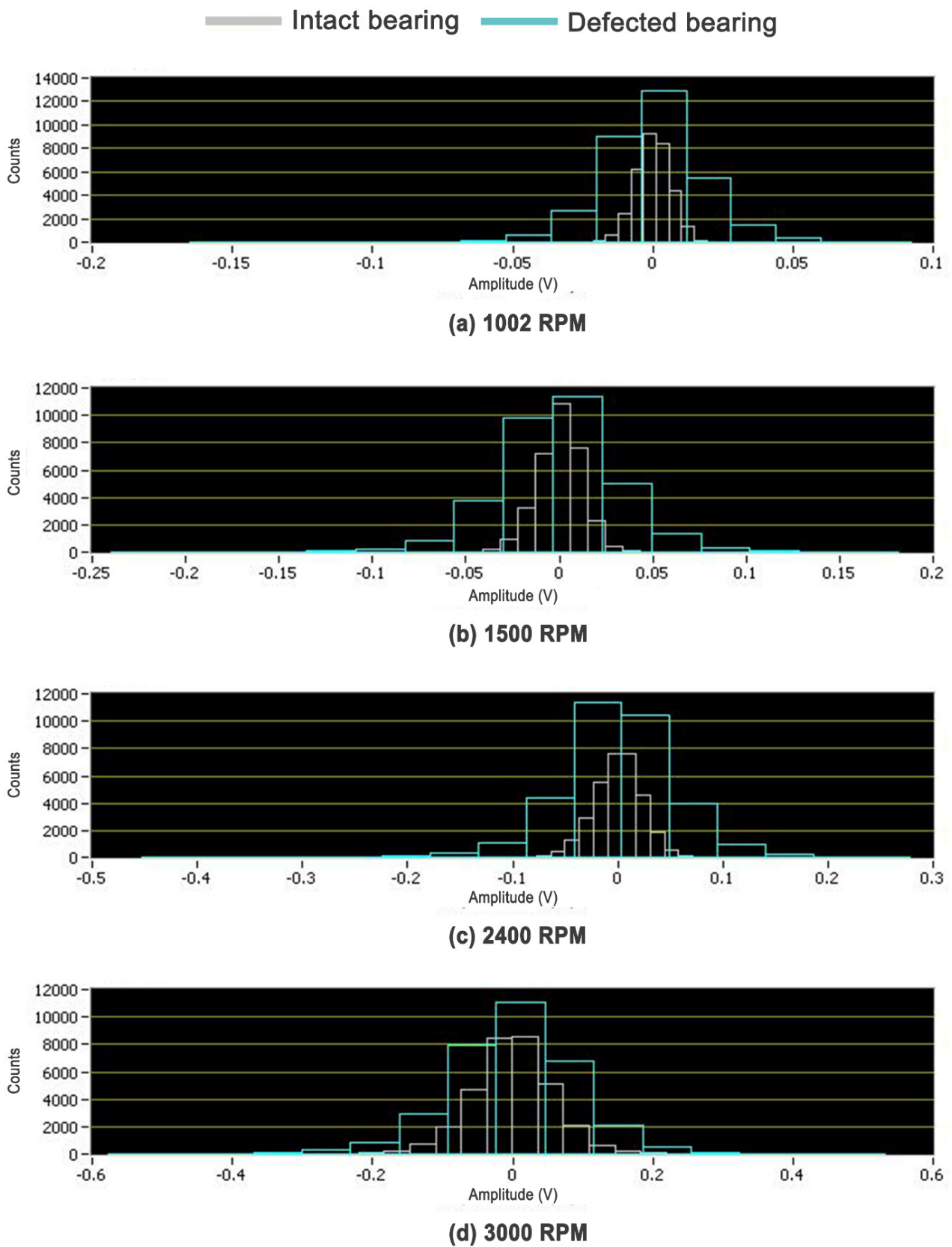


Figure 5. Histograms for an outer race damage with installing a bearing loader.

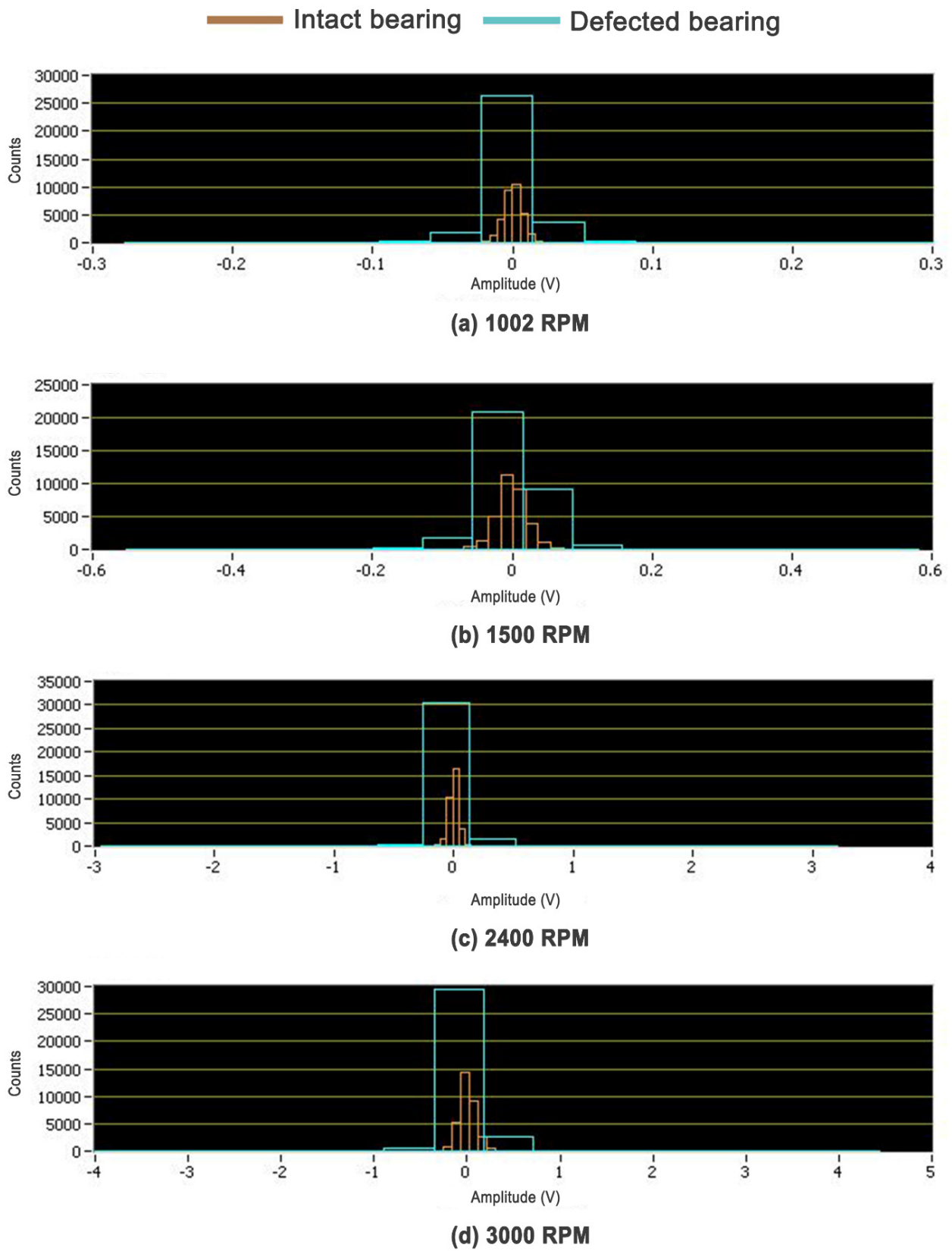


Figure 6. Histograms for ball damage without installing a bearing loader.

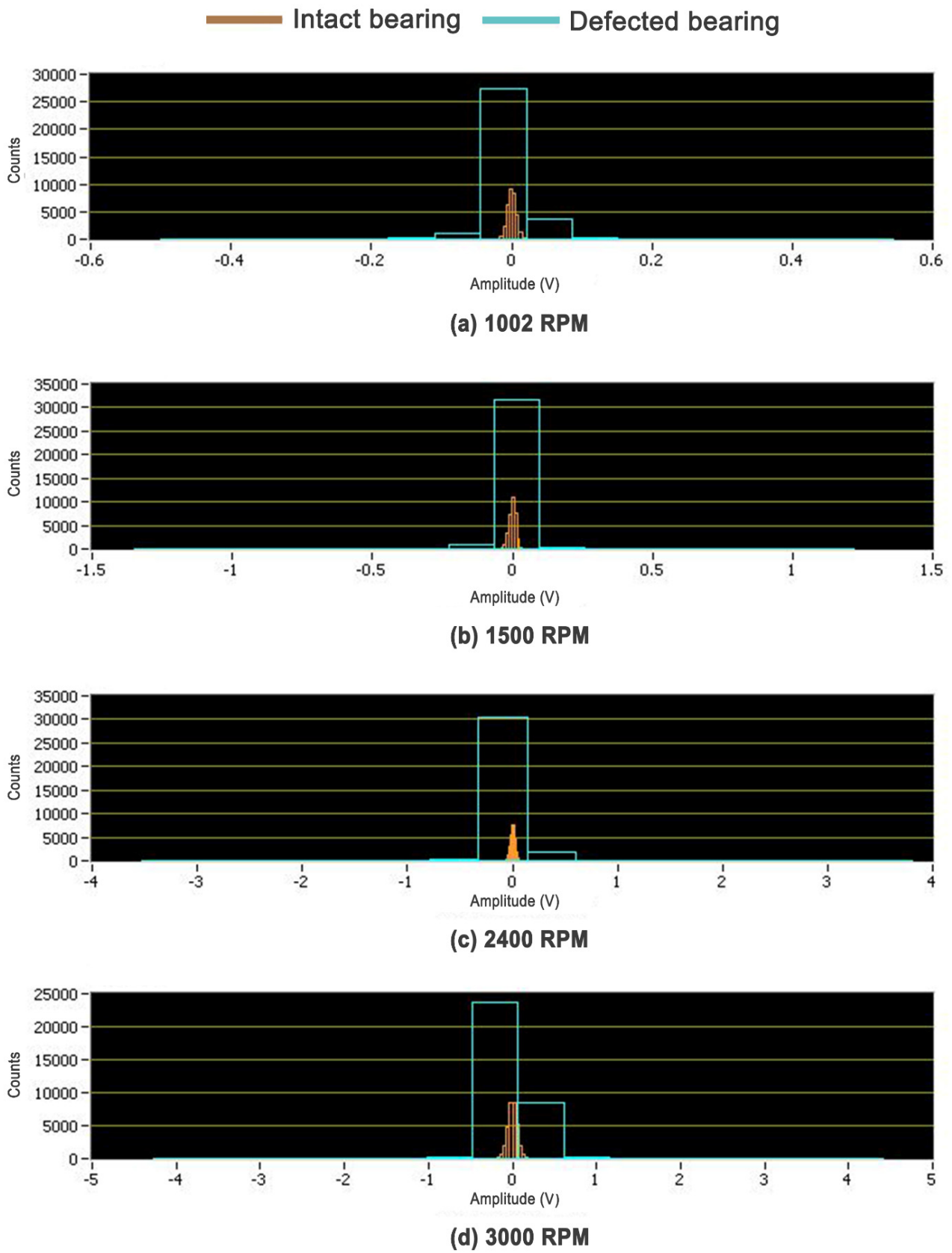


Figure 7. Histograms for ball damage with installing a bearing loader.

Table 6. Averaged kurtosis values for a ball defect.

Rotating Speed (RPM)	Without Installing a Bearing Loader		With Installing a Bearing Loader	
	Intact Bearing	Damaged Bearing	Intact Bearing	Damaged Bearing
1002	2.319673	11.60388	1.609728	18.42259
1500	2.518273	8.712126	1.803017	57.00807
2400	4.293731	42.89402	1.659314	52.58134
3000	2.661141	28.87041	1.920782	38.31863

Figures 6 and 7 reveal that the vibrations are high in case of a ball damaged bearing as compared to the intact bearing. Due to the defect, the bearing produces greater vibrations that result in high bars in the histograms, showing that the damage energy can be a good indicator of faults in roller bearings. The histograms for ball damage, without installing a bearing loader and with installing a bearing loader, are almost the same for all rotating speeds, but the histograms with installing a bearing loader have very high bars due to the fact that with the installation of a bearing loader, the load on the damaged bearing increases, which increase the vibrations. Table 6 clearly shows the high kurtosis values for a ball damaged bearing, as the kurtosis is a measurement of the thickness or heaviness of the tails of a distribution, so it can be said that a ball damaged bearing produces high vibration, which results in high kurtosis values. The histograms and kurtosis values revealed that it is an effective method in detecting the ball fault at an early stage in a roller bearing.

4.4. Combination Defect

For the analysis of the combination defect, an intact bearing was removed, and a combination damaged bearing was mounted in the outboard housing. The vibration data were recorded at four rotating speeds: 1002, 1500, 2400, and 3000 RPM, by mounting the accelerometers at the outboard and inboard bearing housings in the horizontal and vertical direction. The comparisons of histograms for intact and combination damaged bearing have been performed at each rotating speed, with the same two operating conditions. In this study, only the vertical direction outboard bearing housing’s histograms, without installing a bearing loader and with installing a bearing loader, have been shown in Figures 8 and 9, respectively, because they better interpret the fault. The vertical direction outboard bearing housing’s kurtosis values for all speeds have also been calculated and are shown in Table 7.

Table 7. Average kurtosis values for a combination defect.

Rotating Speed (RPM)	Without Installing a Bearing Loader		With Installing a Bearing Loader	
	Intact Bearing	Damaged Bearing	Intact Bearing	Damaged Bearing
1002	2.319673	38.96501	1.609728	8.019885
1500	2.518273	28.0766	1.803017	7.212048
2400	4.293731	12.66049	1.659314	4.472537
3000	2.661141	4.883097	1.920782	4.926638

The histograms for a combination damage, shown in Figures 8 and 9, also depict the same results as the other damages, as it must be the same since we use a combination damaged bearing that is a combination of inner race, outer race, and ball defects. The vibration bars are high for all rotating speeds, and the vibration data are scattered for a damaged bearing without installing a bearing loader, and with installing a bearing loader. The presence of high amplitude vibrations in Figures 8 and 9 for a damaged bearing concluded that histograms, along with the kurtosis values, are highly effective in detecting the roller bearing faults. Without installing the bearing loader, the bars are not much more prominent for a damaged bearing due to the fact that vibrations generated at a smaller load have low amplitudes. The kurtosis values for combination damaged bearings are also high at all rotating speeds, as shown in Table 7. The histograms depicting the vibration data and

kurtosis values clarify the thickness of this vibration data. Hence, the vibration energy at damage-based statistical approach is an excellent technique for the detection of faults in roller bearings.

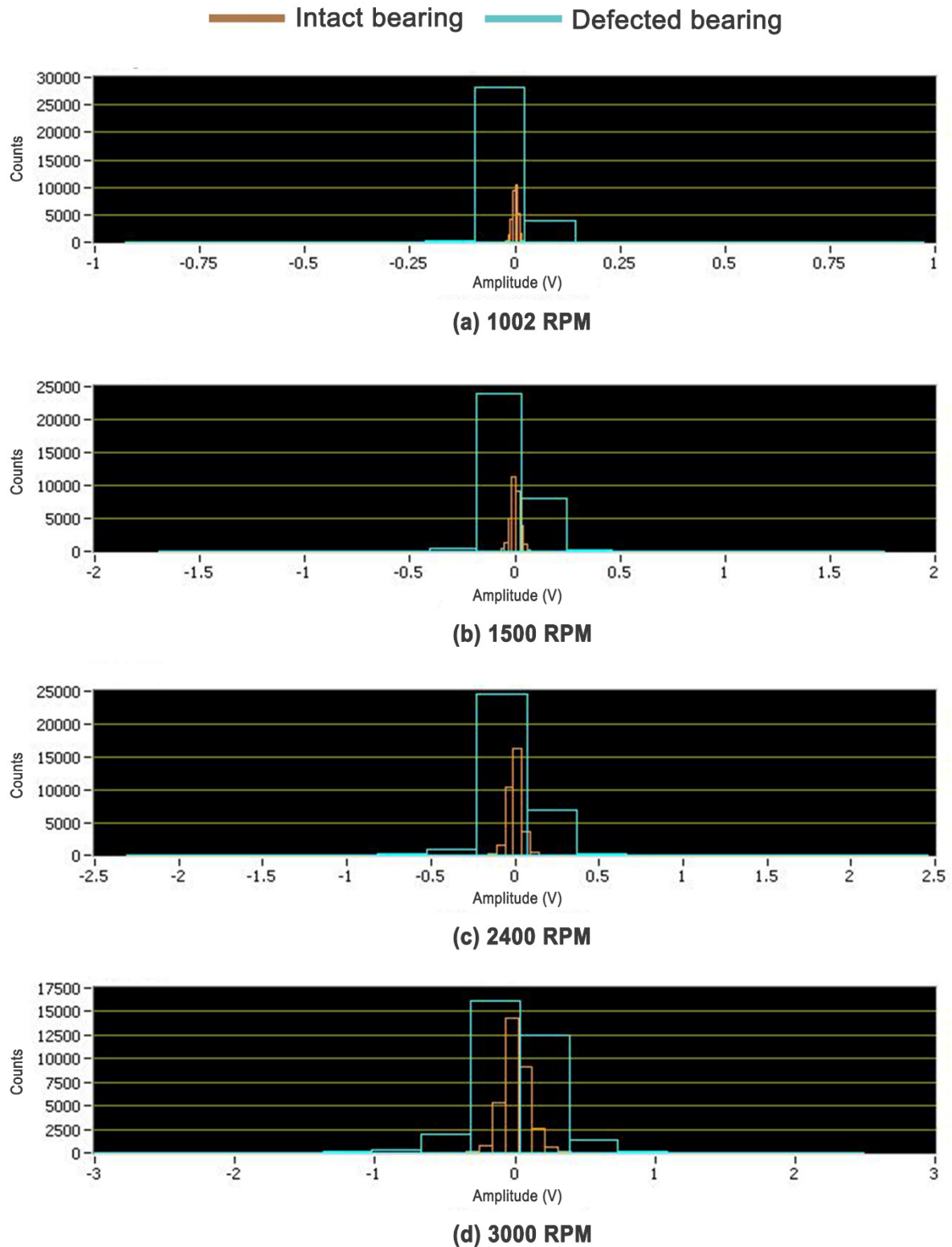


Figure 8. Histograms for a combination of damage without installing a bearing loader.

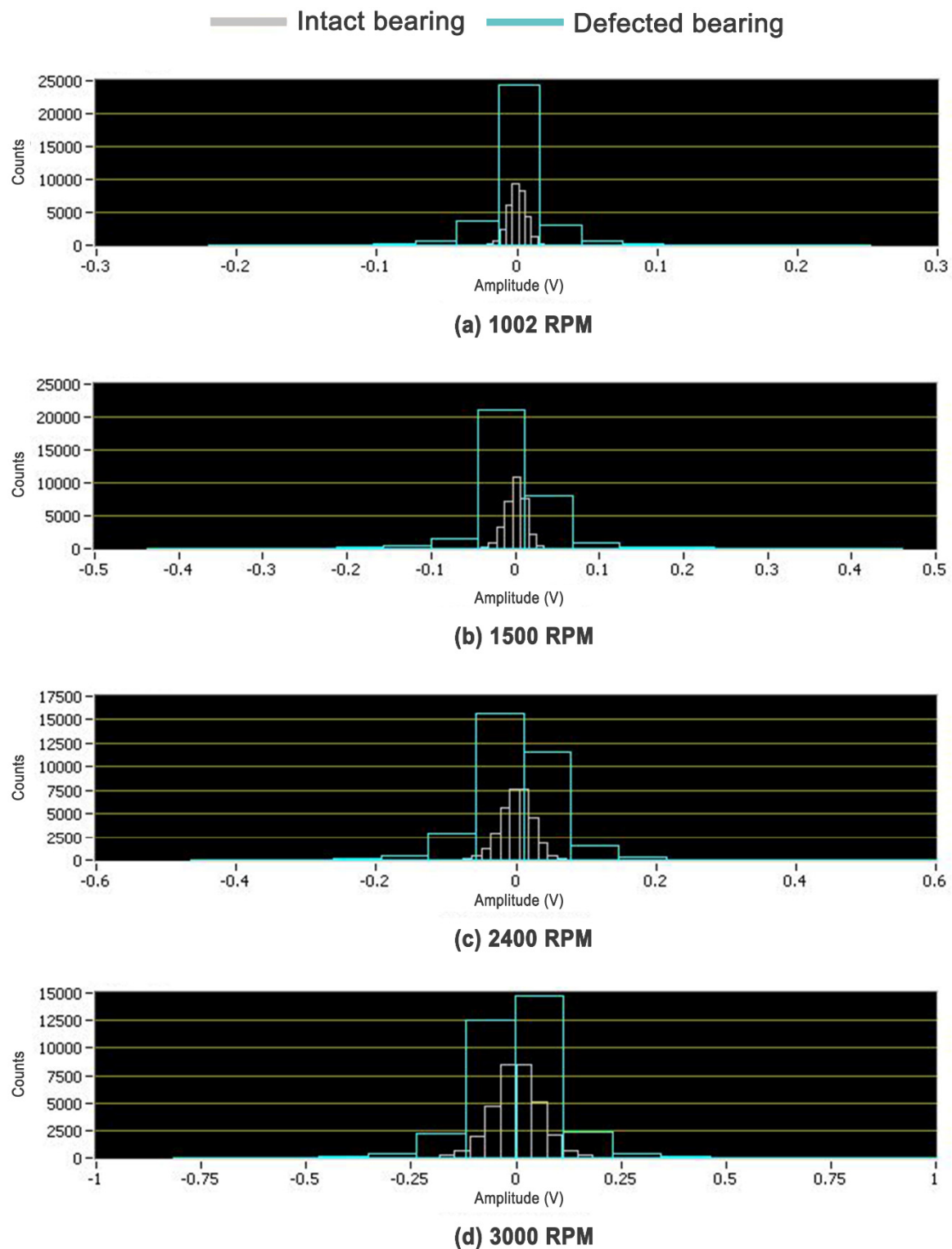


Figure 9. Histograms for a combination of damage with installing a bearing loader.

The comparison of all kurtosis values for all types of damages, without installing a bearing loader and with installing a bearing loader, has also performed in this study, and is shown in Figures 10 and 11, respectively. The kurtosis values shown in Tables 4–7 are used for this comparison. The comparison revealed that the kurtosis values for all types of damages are high as compared to intact bearing, and the results of without installing a bearing loader (Figure 10) give a better understanding of the concept of the vibration

energy at damage-based statistical approach. The results shown in Figure 11 are not clear, but the ball damaged bearing's kurtosis values are higher at each rotating speed.

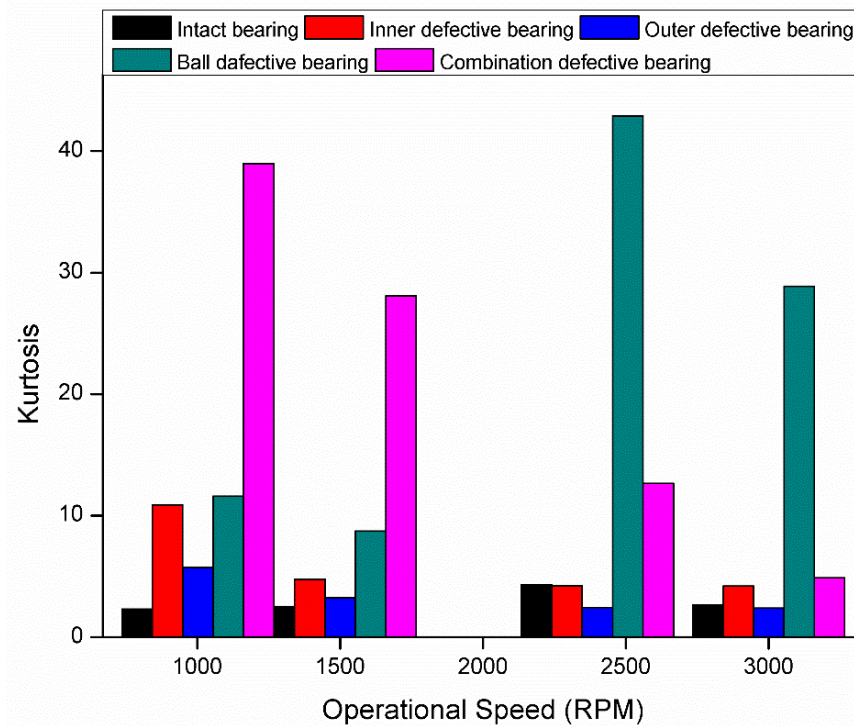


Figure 10. Comparison of averaged kurtosis values without installing a bearing loader.

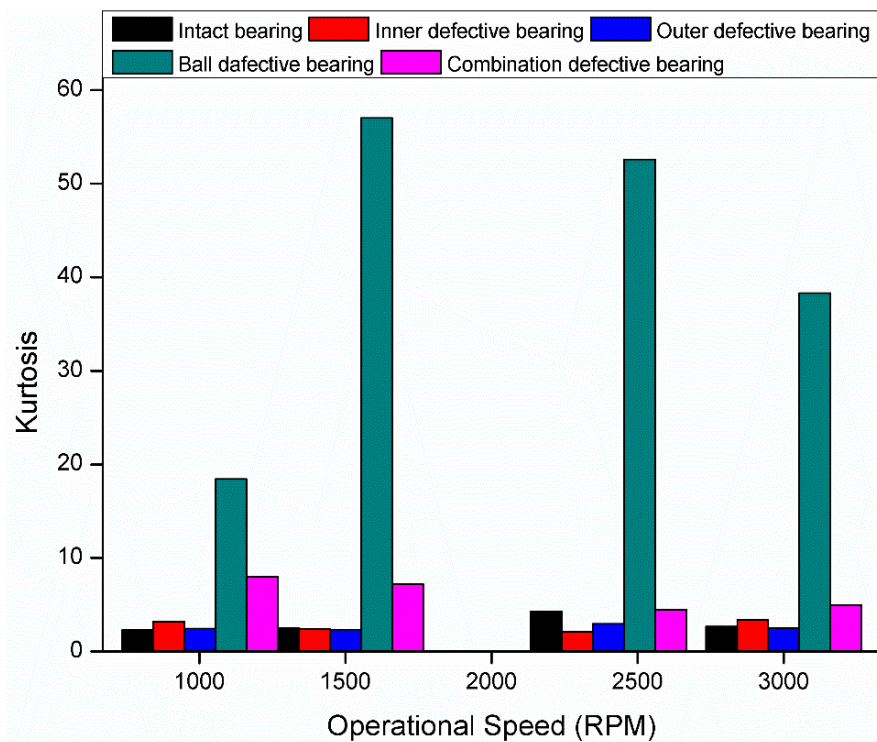


Figure 11. Comparison of averaged kurtosis values with installing a bearing loader.

5. Conclusions

From the above discussion, the following conclusions can be drawn:

1. The vibration bars are high for all rotating speeds, and vibration data are scattered for each damaged bearing for both of the loading conditions—without installing a bearing loader and with installing a bearing loader—due to the fact that the damaged bearing produces high vibrations, as it has high damage energy.
2. The kurtosis values are also high for each damaged bearing and all rotating speeds.
3. The vibration data for an outer race damaged bearing are more scattered as compared to the intact bearing, since the width and height of the bars for an outer race damaged bearing are greater.
4. For some data, without installing the bearing loader, the bars are not prominent for a damaged bearing due to the fact that vibrations generated at a smaller load have lower amplitudes.
5. Due to the defect, damaged bearings produce greater vibrations, resulting in high bars in histograms and showing that the damage energy can be a good indicator to detect faults in roller bearings.
6. As the kurtosis values give a better idea of vibration energy at damage, thus, the histograms and kurtosis values revealed that the energy at damage-based approach is an efficient way to detect damages in the rolling bearing.
7. The comparison of all kurtosis values for all types of damages, without installing a bearing loader and with installing a bearing loader, revealed that the kurtosis values for all types of damages are high as compared to intact bearings, and the results regarding the condition of without installing a bearing loader provide a better understanding of the concept of the vibration energy at damage-based statistical approach.
8. These results are based on the simulator; the real bearing fault detection could be more difficult due to the noise coming from different devices. However, this novel methodology can be helpful in detecting damages at early stages.

Author Contributions: Conceptualization, N.A.; data curation, N.A.; formal analysis, N.A. and A.K.; funding acquisition, X.Y.; investigation, X.Y.; methodology, N.A. and A.K.; project administration, X.Y. and A.K.; resources, X.Y.; software, N.A., A.K. and J.J.; supervision, X.Y. and A.K.; validation, N.A.; writing—original draft, N.A.; writing—review and editing, N.A., X.Y., A.K. and J.J. All authors have read and agreed to the published version of the manuscript.

Funding: This research was funded by the National Natural Science Foundation of China (Grant No. 51105316) and the Natural Science Basic Research Plan in Shaanxi Province of China (Grant No. 2018JM5107).

Institutional Review Board Statement: Not applicable.

Informed Consent Statement: Not applicable.

Data Availability Statement: It is declared that the authors have all the raw data in excel files, and data will be provided upon request.

Conflicts of Interest: The authors declare no conflict of interest.

Abbreviations

ALIF	adaptive local iterative filtering
BPFI	ball pass frequency inner
BPFO	ball pass frequency outer race
BSP	ball spin frequency
CNN	convolutional neural network
DAQ	data acquisition system
DOF	degrees of freedom
EPST	extended phase space topology
FTF	fundamental train frequency
Hz	hertz
IMDE	improved multiscale dispersion entropy (IMDE)
MFS	machinery fault simulator
mRMR	max-relevance min-redundancy
REB	rolling element bearings
TGP	turned, ground, and polished
VR	vibrational resonance

References

- Mobley, R.K. *Maintenance Fundamentals*; Elsevier: Amsterdam, The Netherlands, 2011.
- Li, G.; Tan, J.; Chaudhry, S.S. Industry 4.0 and big data innovations. *Enterp. Inf. Syst.* **2019**, *13*, 145–147. [[CrossRef](#)]
- Sanati, M.; Sandwell, A.; Mostaghimi, H.; Park, S.S. Development of Nanocomposite-Based Strain Sensor with Piezoelectric and Piezoresistive Properties. *Sensors* **2018**, *18*, 3789. [[CrossRef](#)]
- Mishra, D.; Roy, R.B.; Dutta, S.; Pal, S.K.; Chakravarty, D. A review on sensor based monitoring and control of friction stir welding process and a roadmap to Industry 4.0. *J. Manuf. Process.* **2018**, *36*, 373–397. [[CrossRef](#)]
- Xu, L.D.; Duan, L. Big data for cyber physical systems in industry 4.0: A survey. *Enterp. Inf. Syst.* **2019**, *13*, 148–169. [[CrossRef](#)]
- Son, J.; Kang, D.; Boo, D.; Ko, K. An experimental study on the fault diagnosis of wind turbines through a condition monitoring system. *J. Mech. Sci. Technol.* **2018**, *32*, 5573–5582. [[CrossRef](#)]
- Haj Mohamad, T.; Samadani, M.; Nataraj, C. Rolling Element Bearing Diagnostics Using Extended Phase Space Topology. *J. Vib. Acoust. Trans. ASME* **2018**, *140*, 061009. [[CrossRef](#)]
- Yan, X.; Jia, M. Intelligent fault diagnosis of rotating machinery using improved multiscale dispersion entropy and mRMR feature selection. *Knowl. Based Syst.* **2019**, *163*, 450–471. [[CrossRef](#)]
- Dybała, J. Diagnosing of rolling-element bearings using amplitude level-based decomposition of machine vibration signal. *Measurement* **2018**, *126*, 143–155. [[CrossRef](#)]
- Zhu, K.; Chen, L.; Hu, X. Rolling Element Bearing Fault Diagnosis by Combining Adaptive Local Iterative Filtering, Modified Fuzzy Entropy and Support Vector Machine. *Entropy* **2018**, *20*, 926. [[CrossRef](#)]
- Gao, J.; Yang, J.; Huang, D.; Liu, H.; Liu, S. Experimental application of vibrational resonance on bearing fault diagnosis. *J. Braz. Soc. Mech. Sci. Eng.* **2018**, *41*, 6. [[CrossRef](#)]
- Popescu, T.D.; Aiordachioaie, D. Fault detection of rolling element bearings using optimal segmentation of vibrating signals. *Mech. Syst. Signal Process.* **2019**, *116*, 370–391. [[CrossRef](#)]
- Yang, R.; Li, H.; Wang, C.; He, C. Rolling element bearing weak feature extraction based on improved optimal frequency band determination. *Proc. Inst. Mech. Eng. Part C J. Mech. Eng. Sci.* **2019**, *233*, 623–634. [[CrossRef](#)]
- Sun, X.; Tan, J.; Wen, Y.; Feng, C. Rolling bearing fault diagnosis method based on data-driven random fuzzy evidence acquisition and Dempster–Shafer evidence theory. *Adv. Mech. Eng.* **2016**, *8*, 1687814015624834. [[CrossRef](#)]
- Zair, M.; Rahmoune, C.; Benazzouz, D. Multi-fault diagnosis of rolling bearing using fuzzy entropy of empirical mode decomposition, principal component analysis, and SOM neural network. *Proc. Inst. Mech. Eng. Part C J. Mech. Eng. Sci.* **2018**, *233*, 3317–3328. [[CrossRef](#)]
- Wang, B.; Hu, X.; Wang, W.; Sun, D. Fault diagnosis using improved pattern spectrum and fruit fly optimization algorithm–support vector machine. *Adv. Mech. Eng.* **2018**, *10*, 1687814018810935. [[CrossRef](#)]
- Hoang, D.-T.; Kang, H.-J. Rolling element bearing fault diagnosis using convolutional neural network and vibration image. *Cogn. Syst. Res.* **2019**, *53*, 42–50. [[CrossRef](#)]
- Abboud, D.; Elbadaoui, M.; Smith, W.A.; Randall, R.B. Advanced bearing diagnostics: A comparative study of two powerful approaches. *Mech. Syst. Signal Process.* **2019**, *114*, 604–627. [[CrossRef](#)]
- Karioja, K.; Lahdelma, S.; Litak, G.; Ambroźkiewicz, B. Extracting periodically repeating shocks in a gearbox from simultaneously occurring random vibration. In Proceedings of the 15th International Conference on Condition Monitoring and Machinery Failure Prevention Technologies, CM/MFPT, Nottingham, UK, 10–12 September 2018; pp. 456–464.
- Ho, D.; Randall, R.B. Optimisation of Bearing Diagnostic Techniques Using Simulated and Actual Bearing Fault Signals. *Mech. Syst. Signal Process.* **2000**, *14*, 763–788. [[CrossRef](#)]

21. Randall, R.B.; Antoni, J.; Chobsaard, S. The Relationship between Spectral Correlation and Envelope Analysis in the Diagnostics of Bearing Faults and Other Cyclostationary Machine Signals. *Mech. Syst. Signal Process.* **2001**, *15*, 945–962. [[CrossRef](#)]
22. Antoni, J.; Randall, R.B. A Stochastic Model for Simulation and Diagnostics of Rolling Element Bearings with Localized Faults. *J. Vib. Acoust. Trans. ASME* **2003**, *125*, 282–289. [[CrossRef](#)]
23. Antoni, J. Cyclic spectral analysis of rolling-element bearing signals: Facts and fictions. *J. Sound Vib.* **2007**, *304*, 497–529. [[CrossRef](#)]
24. Meier, N.; Ambrozkiewicz, B.; Georgiadis, A.; Litak, G. Verification of measuring the bearing clearance using kurtosis, recurrences and neural networks and comparison of these approaches. In Proceedings of the 2019 IEEE SENSORS, Montreal, QC, Canada, 27–30 October 2019; pp. 1–4.
25. Azeem, N.; Yuan, X. Experimental study on the Condition Monitoring of Shaft Unbalance by using Vibrations Spectrum and phase Analysis. In Proceedings of the 7th International Conference on Condition Monitoring and Diagnosis, CMD 2018, Perth, WA, Australia, 23–26 September 2018; pp. 1–6.
26. Azeem, N.; Yuan, X.; Raza, H.; Urooj, I. Experimental condition monitoring for the detection of misaligned and cracked shafts by order analysis. *Adv. Mech. Eng.* **2019**, *11*, 1687814019851307. [[CrossRef](#)]
27. Azeem, N.; Yuan, X.; Urooj, I.; Jabbar, J. Vibration-based Power Spectral Density Analysis for the Detection of Multiple Faults in Rolling Element Bearings. In Proceedings of the 2019 5th International Conference on Control, Automation and Robotics (ICCAR), Beijing, China, 19–22 April 2019; pp. 719–726.
28. Azeem, N.; Yuan, X.; Urooj, I.; Jabbar, J. An Octave Analysis Approach Based on Vibrational Data for Early Detection of Multiple Faults in Rolling Bearing. In Proceedings of the 2019 5th International Conference on Control, Automation and Robotics (ICCAR), Beijing, China, 19–22 April 2019; pp. 560–565.
29. Gama, A.L.; de Lima, W.B.; de Veneza, J.P.S. Detection of Shaft Misalignment Using Piezoelectric Strain Sensors. *Exp. Tech.* **2017**, *41*, 87–93. [[CrossRef](#)]
30. Fatima, S.; Dastidar, S.G.; Mohanty, A.R.; Naikan, V.N.A. Technique for optimal placement of transducers for fault detection in rotating machines. *Proc. Inst. Mech. Eng. Part O-J. Risk Reliab.* **2013**, *227*, 119–131. [[CrossRef](#)]
31. *ISO 20816-1:2016*; Mechanical Vibration—Measurement and Evaluation of Machine Vibration—Part 1: General Guidelines. International Organization for Standardization: Geneva, Switzerland, 2016.